Exact solution of the boundary-dissipated transverse field Ising model: Structure of the Liouvillian spectrum and dynamical duality

Zhen-Yu Zheng [1,*] Xueliang Wang,[1,2,*] and Shu Chen [1,2,3,†]

[1]*Beijing National Laboratory for Condensed Matter Physics, Institute of Physics, Chinese Academy of Sciences, Beijing 100190, China*
[2]*School of Physical Sciences, University of Chinese Academy of Sciences, Beijing 100049, China*
[3]*Yangtze River Delta Physics Research Center, Liyang, Jiangsu 213300, China*

We study the boundary-dissipated transverse field Ising model described by a Lindblad master equation and exactly solve its Liouvillian spectrum in the whole parameter space. By mapping the Liouvillian into a Su-Schrieffer-Heeger model with imaginary boundary potentials under a parity constraint, we solve the rapidity spectrum analytically and thus construct the Liouvillian spectrum strictly with a parity constraint condition. Our results demonstrate that the Liouvillian spectrum displays four different structures, which are characterized by different numbers of segments. By analyzing the properties of rapidity spectrum, we can determine the phase boundaries between different spectrum structures analytically and prove the Liouvillian gap fulfilling a duality relation in the weak and strong dissipation region. Furthermore, we unveil the existence of a dynamical duality, i.e., the long-time relaxation dynamics exhibits almost the same dynamical behavior in the weak and strong dissipation region as long as the duality relation holds true.

I. INTRODUCTION

Advances in quantum engineering of dissipation in laboratory have attracted a growing interest in the study of open quantum systems in engineered condensed matter systems [1–3], among which a particularly important class is the boundary-driven system, where the system is coupled to the environment only at the boundaries. Within the Markovian approximation, the dynamic evolution process of a boundary-driven quantum system is governed by the Lindblad master equation [4] with the influence of environment described by boundary dissipation operators. Understanding dynamical processes driven by boundary dissipations have attracted intensive theoretical studies [5–17].

As a paradigmatic system exhibiting quantum phase transition, the transverse field Ising model is exactly solvable and has been well studied in the past decades [18–22]. However, much less is understood for the corresponding boundary-dissipation-driven model. Recently, exactly solvable dissipative models have attracted many interests [9–12,23–26]. Usually, the solvability of these models mainly relies on free-fermion (boson) techniques or Bethe-ansatz method. One specific class that has been widely studied is the open quantum systems with quadratic Lindbladian, which can be solved by third quantization [7–12]. Although the third quantization method can reduce the problem of solving quadratic Lindbladian to the diagonalization of a non-Hermitian matrix, analytical solutions are still limited except for some specific cases or for a special set of parameters [11–13]. The calculation of full Liouvillian spectrum and understanding the spectrum structure in the whole parameter space is still a challenging work.

In this work, we shall present an exact solution to a transverse field Ising chain with boundary dissipations in the whole parameter space and construct the Liouvillian spectrum from the rapidity spectrum under the constraint of parity. By vectorizing the density matrix, solving the Lindblad master equation with boundary dissipation can be mapped to the solution of the Su-Schrieffer-Heeger (SSH) model with imaginary boundary potentials [27], which enables us to obtain analytical results of the rapidity spectrums. We stress that the Liouvillian spectrum can be constructed correctly only when the constraint of parity is properly taken into account. Focusing on the case with equal boundary dissipations, we demonstrate that the Liouvillian spectrum displays four different structures in the whole parameter space. We unveil that the different structures of the Liouvillian spectrum are determined by number of the complex solutions of equation for solving eigenvalues of the odd-parity rapidity spectrum. The boundaries between different regions can be analytically determined via a theoretical analysis in the thermodynamical limit. Furthermore, we prove that the Liouvillian gap fulfills a dual relation in the weak and strong dissipation region and uncover the existence of a dynamical duality of the relaxation dynamics. Our work demonstrates novel phenomena of dynamical duality from the perspective of an exact solution and provides a firm ground for understanding structure of Liouvillian spectrum [24,28].

The paper is organized as follows. In Sec. II, we rigorously establish the mapping relation between the model and the non-Hermitian matrices associated with parity and emphasize the importance of both even and odd parity. In Sec. III, we

---

*These authors contributed equally to this work.

†schen@iphy.ac.cn

024404-1

solve the rapidity spectrum analytically and construct the Liouvillian spectrum via the rapidity spectrum under the parity constraint. Focusing on the case with equal boundary dissipation strengthes, we demonstrate that the Liouvillian spectrum has four different structures. In Sec. IV, we investigate the Liouvillian gap and the relaxation dynamics and unveil the existence of a dynamical duality. A summary is given in Sec. V.

II. MODEL AND FORMALISM

We consider the boundary-dissipated open system with the time evolution of the density matrix ρ described by the Lindblad equation:

$$
\frac{d\rho}{dt} = \mathcal{L}[\rho] := -i[H, \rho] + \sum_\mu \left(L_\mu \rho L_\mu^\dagger - \frac{1}{2}\{L_\mu^\dagger L_\mu, \rho\} \right),
\tag{1}
$$

where we have set $\hbar = 1$, and H is the Hamiltonian governing the unitary part of dynamics of the system described by a transverse field Ising chain [19,21]:

$$
H = -J \sum_{j=1}^{N-1} \sigma_j^x \sigma_{j+1}^x - h \sum_{j=1}^{N} \sigma_j^z.
\tag{2}
$$

Here N is the total number of lattice sites and $\sigma_j^\alpha (j = 1, \ldots, N, \alpha = x, y, z)$ are Pauli matrices at per site. The dissipative processes are described by the Lindblad operators L_μ with the index μ denoting the dissipation channels. Here we consider that the dissipations appear at left and right edges, i.e.,

$$
L_L = \sqrt{\gamma_L}\sigma_1^x, \quad L_R = \sqrt{\gamma_R}\sigma_N^x,
\tag{3}
$$

where $\gamma_L, \gamma_R \geqslant 0$ denote the boundary dissipation strengths. Here we take $\gamma_L = \gamma_R = \gamma$ and set $J = 1$ as the energy units.

The Liouvillian $\mathcal{L}$ is a superoperator acting in the space of density matrix operators.

By using the Choi-Jamiolkwski isomorphism [29–33], the density matrix is mapped into a vector:

$$
\rho = \sum_{mn} \rho_{mn}|m\rangle\langle n| \ \rightarrow \ |\rho\rangle = \sum_{mn} \rho_{mn}|m\rangle \otimes |n\rangle,
$$

and thus the Liouvillian can be expressed by the $4^N \times 4^N$ matrix,

$$
\mathcal{L} \cong i(\mathbf{1} \otimes H^T - H \otimes \mathbf{1})
$$
$$
+ \sum_i \left[L_i \otimes L_i^* - \frac{1}{2}\left(L_i^\dagger L_i \otimes \mathbf{1} + \mathbf{1} \otimes L_i^T L_i^* \right) \right],
\tag{4}
$$

which gives rise to

$$
\mathcal{L} = i\left(J \sum_{j=1}^{N-1} \sigma_j^x \sigma_{j+1}^x + h \sum_{j=1}^{N} \sigma_j^z - J \sum_{j=1}^{N-1} \tau_j^x \tau_{j+1}^x - h \sum_{j=1}^{N} \tau_j^z \right)
$$
$$
+ \gamma_L \sigma_1^x \tau_1^x + \gamma_R \sigma_N^x \tau_N^x - (\gamma_L + \gamma_R).
\tag{5}
$$

By using the Jordan-Wigner transformation [13],

$$
a_j = (-1)^j \left(\prod_{i=1}^{j-1} \sigma_i^z \right) \sigma_j^x,
$$

$$
b_j = (-1)^j \left(\prod_{i=1}^{j-1} \sigma_i^z \right) \sigma_j^y,
$$

$$
\bar{a}_j = (-1)^j \left(\prod_{i=1}^{N} \sigma_j^i \right) \left(\prod_{i=1}^{N-j} \tau_{N+1-i}^z \right) \tau_j^x,
$$

$$
\bar{b}_j = (-1)^{j-1} \left(\prod_{i=1}^{N} \sigma_j^i \right) \left(\prod_{i=1}^{N-j} \tau_{N+1-i}^z \right) \tau_j^y,
\tag{6}
$$

it follows that the Liouvillian $\mathcal{L}$ can be represented as

$$
\mathcal{L} = -h \sum_{j=1}^{N} (a_j b_j + \bar{a}_j \bar{b}_j) + J \sum_{j=1}^{N-1} (b_j a_{j+1} + \bar{b}_{j+1} \bar{a}_j)
$$
$$
+ i\mathcal{P}(\gamma_L \bar{b}_1 a_1 + \gamma_R b_N \bar{a}_N) - (\gamma_L + \gamma_R),
\tag{7}
$$

where a_j, b_j, $\bar{a}_j$, and $\bar{b}_j$ are Majorana fermion operators. Here $\mathcal{P}$ is the parity operator defined as

$$
\mathcal{P} := \left(\prod_{j=1}^{N} \sigma_j^z \right) \left(\prod_{j=1}^{N} \tau_j^z \right).
\tag{8}
$$

The eigenvalue of the parity operator $\mathcal{P}$ takes a specific value with $P = \pm 1$. It can be checked $[\mathcal{L}, \mathcal{P}] = 0$. When $P = -1$, the Liouvillian $\mathcal{L}$ is in the operator space with odd parity, whereas $P = 1$ corresponds to the operator space with even parity. We notice that the parity operator $\mathcal{P}$ gives a strong constraint on the mapping between the spin Hilbert space and the fermionic Hilbert space. Because the total degrees of freedom of the Liouvillian with odd parity $\mathcal{L}^P|_{P=-1}$ and even parity $\mathcal{L}^P|_{P=1}$ is twice as the degrees of freedom of the Liouvillian $\mathcal{L}$, this gives rise to redundant degrees of freedom. To eliminate the redundant degrees of freedom, we apply the projection and the mapping relation as follows:

$$
\mathcal{L} = P^+ \mathcal{L}^P|_{P=1} P^+ + P^- \mathcal{L}^P|_{P=-1} P^-,
\tag{9}
$$

where the projectors are defined as

$$
P^\pm = \tfrac{1}{2}(1 \pm \mathcal{P}).
\tag{10}
$$

For convenience, we use the creation operator and the annihilation operator of fermions, defined as

$$
a_j = c_{2j-1} + c_{2j-1}^\dagger, \quad \bar{b}_j = \frac{1}{i}(c_{2j-1} - c_{2j-1}^\dagger),
\tag{11}
$$

$$
\bar{a}_j = c_{2j} + c_{2j}^\dagger, \quad b_j = \frac{1}{i}(c_{2j} - c_{2j}^\dagger),
\tag{12}
$$

to rewrite the Liouvillian as

$$
\mathcal{L}^P = 2i\left[h \sum_{j=1}^{N} (c_{2j-1}^\dagger c_{2j} + \text{H.c.}) + J \sum_{j=1}^{N-1} (c_{2j}^\dagger c_{2j+1} + \text{H.c.}) \right]
$$
$$
- 2\gamma_L P \left(c_1^\dagger c_1 - \frac{1}{2} \right) - 2\gamma_R \left(c_{2N}^\dagger c_{2N} - \frac{1}{2} \right) - (\gamma_L + \gamma_R)
$$
$$
= 2i\mathbf{c}^\dagger T^P \mathbf{c} + \gamma_L(P - 1),
\tag{13}
$$

where the spinors are denoted as $\mathbf{c}^\dagger = (c_1^\dagger, \ldots, c_{2N}^\dagger)$, $\mathbf{c} = (c_1, \ldots, c_{2N})^T$, and T^P is represented in terms of a $2N \times 2N$ non-Hermitian matrix as follows:

$$
T^P = \begin{pmatrix}
Pi\gamma_L & h & \cdots & \cdots & & 0 \\
h & 0 & J & & & \\
& J & 0 & \ddots & & \\
& & \ddots & \ddots & \ddots & \\
& & & \ddots & 0 & h \\
0 & \cdots & \cdots & & h & i\gamma_R
\end{pmatrix}. \tag{14}
$$

In terms of fermion operator, the parity operator is represented as $\mathcal{P} = (-1)^{\hat{N}_f}$ with $\hat{N}_f = \sum_{j=1}^{2N} c_j^\dagger c_j$ being the total complex fermion number operator. The parity of the Liouvillian $\mathcal{L}$ corresponds to the total number of complex fermions being even or odd, with $P = 1$ and -1 corresponding to the even and odd parity, respectively. For the case with $\gamma_L = \gamma_R = \gamma$, the Liouvillian with a specific parity is written as

$$
\mathcal{L}^P = 2i\mathbf{c}^\dagger T^P \mathbf{c} + \gamma(P - 1), \tag{15}
$$

where T^P is given by

$$
T^P = \begin{pmatrix}
Pi\gamma & h & \cdots & \cdots & & 0 \\
h & 0 & 1 & & & \\
& 1 & 0 & \ddots & & \\
& & \ddots & \ddots & \ddots & \\
& & & \ddots & 0 & h \\
0 & \cdots & \cdots & & h & i\gamma
\end{pmatrix}. \tag{16}
$$

Here we have set $J = 1$. It is clear that T^P describes a non-Hermitian SSH model [34] with imaginary boundary potentials [13,27,35].

By using the eigen-decomposition $T^P = \sum_{j=1}^{2N} E_{j,P} |\Psi_{j,P}\rangle \langle \Phi_{j,P}|$, we can get the diagonal form of the Liouvillian:

$$
\mathcal{L}^P = 2i \sum_{j=1}^{2N} E_{j,P} \overline{d}_{j,P} d_{j,P} + \gamma(P - 1), \tag{17}
$$

where $d_{j,P} = \sum_{i=1}^{2N} \zeta_{j,P,i} c_i$ and $\overline{d}_{j,P} = \sum_{i=1}^{2N} \xi_{j,P,i} c_i^\dagger$. The parameters $\xi_{j,P,i}$ and $\zeta_{j,P,i}$ are the ith element of $|\Psi_{j,P}\rangle$ and $\langle \Phi_{j,P}|$, respectively. Here we take the Bogoliubov modes as $(d_{j,P}, \overline{d}_{j,P})$ instead of $(d_{j,P}, d_{j,P}^\dagger)$, which satisfy the canonical anticommutation relations [36,37]

$$
\{d_{j,P}, \overline{d}_{j',P}\} = \delta_{jj'},
$$
$$
\{d_{j,P}, d_{j',P}\} = \{\overline{d}_{j,P}, \overline{d}_{j',P}\} = 0.
$$

According to Eq. (9), the eigenstates of the Liouvillian $\mathcal{L}$ comes from two parts which contain all occupied states of even complex fermions from $\mathcal{L}^P|_{P=1}$ and of odd complex fermions from $\mathcal{L}^P|_{P=-1}$. Thus, we can get the full eigenstates and the spectrum of Liouvillian $\mathcal{L}$ by the reorganizations of the rapidity spectrum of $\mathcal{L}^P|_{P=1}$ and $\mathcal{L}^P|_{P=-1}$.

III. STRUCTURE OF LIOUVILLIAN SPECTRUM

The full spectrum of Liouvillian $\mathcal{L}$ can be obtained by reorganizing the rapidity spectrum of $\mathcal{L}^P|_{P=1}$ and $\mathcal{L}^P|_{P=-1}$, which can be analytically derived by solving the eigenvalues of T^P, i.e.,

$$
T^P \Psi_P = E_P \Psi_P, \tag{18}
$$

where Ψ_P denotes the eigenvector corresponding to the eigenvalue E_P (the rapidity spectrum). We can exactly solve the eigenvalues by applying the analytical method in Ref. [38]. In terms of the parameter θ, the eigenvalue can be represented as

$$
E_P = \pm\sqrt{1 + h^2 + 2h\cos\theta}. \tag{19}
$$

The value of θ is determined by the boundary equations [38], which leads to the following equation (the details are shown in Appendix A):

$$
p_1 \sin[N\theta] - p_2 \sin[(N+1)\theta] + p_3 \sin[(N-1)\theta] = 0, \tag{20}
$$

where $p_1 = i(P + 1)\gamma E_P - (1 - P\gamma^2)$, $p_2 = h$, and $p_3 = hP\gamma^2$.

By solving Eq. (20), we can obtain the value of θ_j and thus the rapidity spectrum. Explicitly, we rewrite Eq. (20) in even channel ($P = 1$) and odd channel ($P = -1$) as

$$
[2i\gamma E_e - (1 - \gamma^2)]\sin[N\theta] - h\sin[(N+1)\theta]
$$
$$
+ h\gamma^2 \sin[(N-1)\theta] = 0, \tag{21}
$$

and

$$
(1 + \gamma^2)\sin[N\theta] + h\sin[(N+1)\theta]
$$
$$
+ h\gamma^2 \sin[(N-1)\theta] = 0, \tag{22}
$$

respectively. For convenience, we denote the solutions of Eq. (21) as θ_e and of Eq. (22) as θ_o, respectively. Substituting them into the formula of eigenvalue in Eq. (19), we can get the rapidity spectrum, denoted as $E_{j,e}$ and $E_{j,o}$ which are eigenvalues of T^e and T^o, respectively, with $j = 1, \ldots, 2N$. By considering the constraint of the parity operator and Eq. (9), the full spectrum of the Liouvillian $\mathcal{L}$ can be exactly expressed as

$$
\lambda = \begin{cases}
2i \sum_{j=1}^{2N} v_{j,e} E_{j,e} & (v_{j,e} = 0, 1), \\
2i \sum_{j=1}^{2N} v_{j,o} E_{j,o} - 2\gamma & (v_{j,o} = 0, 1),
\end{cases} \tag{23}
$$

where $\sum_{j=1}^{2N} v_{j,e}$ is even and $\sum_{j=1}^{2N} v_{j,o}$ is odd. The constraint on the total complex fermion number removes the redundant degrees of freedom.

In Fig. 1 we demonstrate the Liouvillian spectrum and the corresponding rapidity spectrum for four typical cases. The rapidity spectrum is obtained by numerically solving Eqs. (21) and (22) and thus the Liouvillian spectrum is obtained from Eq. (23). The Liouvillian spectrum displays different structures in the four parameter regions, as schematically displayed in Fig. 2. We have checked our Liouvillian spectra by comparing with the numerical results via the diagonalization of Liouvillian and find that they agree exactly.

We observe that the Liouvillian spectrums from the odd channel present distinct stripes and from the even channel are scattered near these stripes, as shown in Figs. 1(a1)–1(a4). For
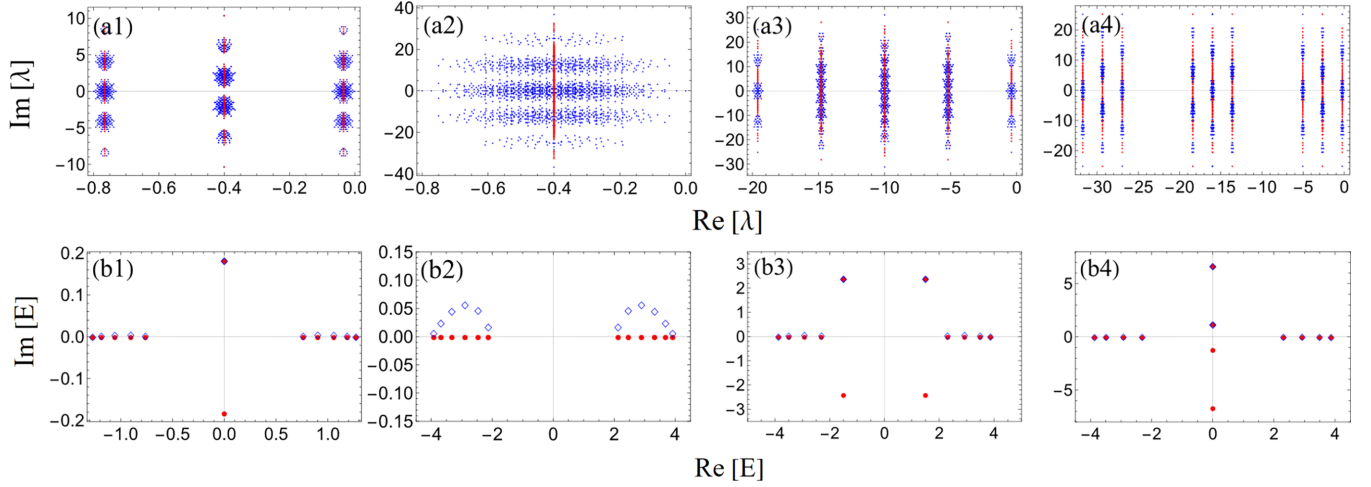
FIG. 1. The Liouvillian spectrum and the rapidity spectrum with $N = 6$, and (a1, b1) $h = 0.3$, $\gamma = 0.2$, and (a2, b2) $h = 3$, $\gamma = 0.2$, and (a3, b3) $h = 3$, $\gamma = 5$, and (a4, b4) $h = 3$, $\gamma = 8$. The red points represent the Liouvillian spectrum of odd channel with $P = -1$, while the blue ones represent that of even channel with $P = 1$. The Liouvillian spectrum in panels (a1, a2, a3, a4) can be constructed by the rapidity spectrum in panels (b1, b2, b3, b4), respectively. The eigenvalues of Liouvillian spectrum in panels (a1, a2, a3, a4) satisfy $\Re[\lambda] \leqslant 0$ and the data of Liouvillian spectrum are consistent with ones by exact diagonalization. The red points in (b1, b2, b3, b4) represent the rapidity spectrum from odd channel and the blue empty prisms represent the rapidity spectrum from even channel.

convenience, we call one stripe and points surrounding this stripe as one segment. The distance between each segment is determined by the imaginary part of rapidity spectrum of the odd channel, and the width of the segments is determined by the imaginary part of rapidity spectrum of the even channel close to the real axis. The number of segments is closely related to number of complex solutions of the rapidity spectrum of the odd channel, which correspond to the boundary bound states of T^o [27]. Since T^o fulfills $\mathscr{PT}$ (parity and time-reversal) symmetry, solutions of Eq. (22) are either real

or occur in complex conjugated pairs. In the $\mathscr{PT}$-symmetry region of $h > 1$ and $\gamma < 1$, all N solutions of Eq. (22) are real. The corresponding rapidity spectrum has no pure imaginary eigenvalues, and the Liouvillian spectrum displays a structure composed of one segment. In the region of $h < 1$, the odd rapidity spectrum has one pair of purely imaginary eigenvalues [see Fig. 1(b1) and Figs. 3(a1) and 3(b1)], and the Liouvillian spectrum is composed of three segments. For
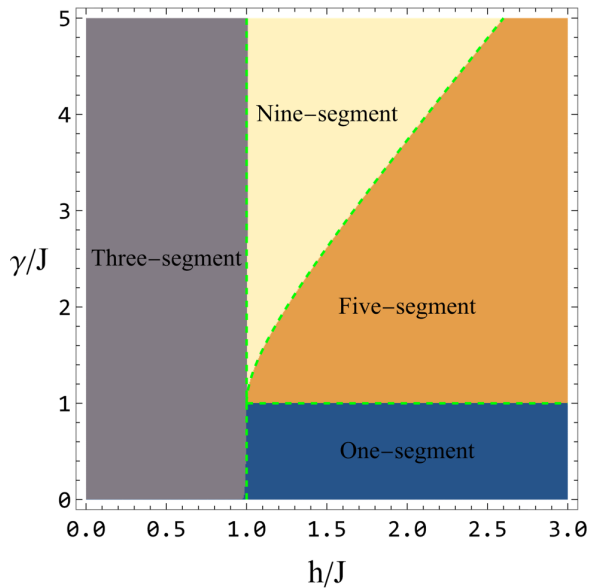

FIG. 2. The schematic phase diagram for the structure of the Liouvillian spectrum. The green dashed lines denote the boundaries between different regions with different number of eigenvalue segments.
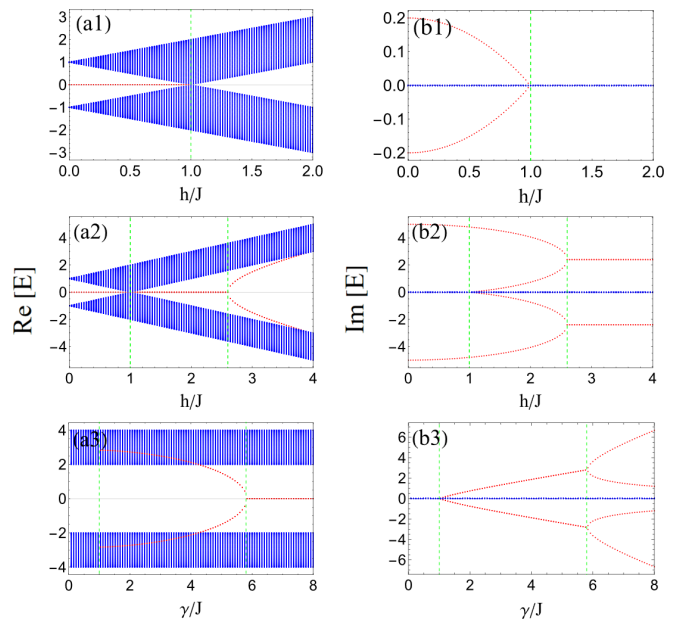

FIG. 3. The rapidity spectrum from the odd channel. The red lines denotes the nonreal roots and green dash lines indicate the boundaries of regions with different complex solutions. We set the parameters with (a1, b1) $N = 100$, $\gamma = 0.2$, (a2, b2) $N = 100$, $\gamma = 5$, and (a3, b3) $N = 100$, $h = 3$.

$h > \frac{1+\gamma^2}{2\gamma}$ and $\gamma > 1$, the odd rapidity spectrum has two conjugated pairs of complex eigenvalues which are symmetrical about the imaginary axis [see Fig. 1(b3) and Figs. 3(a3) and 3(b3)], and the Liouvillian spectrum displays a structure of five segments. For $h = 3$ and $\gamma = 8$, the odd rapidity spectrum has two conjugated pairs of purely imaginary eigenvalues, inducing that the Liouvillian spectrum presents a structure of nine segments.

For the even channel, T^e fulfills the reflection symmetry and K symmetry. The corresponding solutions of Eq. (21) are complex and distribute symmetrically about the imaginary axis (see Appendix A for details). As shown in Figs. 1(b1)–1(b4), the rapidity spectrum from the even channel has a one-to-one correspondence to the spectrum from the odd channel. For the eigenvalues close to the real axis, their imaginary part determines the width of the segments in the Liouvillian spectrum. There also exist complex eigenvalues farther away from the real axis, which are degenerate and almost overlap with one (ones) of the corresponding complex conjugated pairs (in the upper half-plane) from the odd channel, as shown in Figs. 1(b1), 1(b3), and 1(b4). Similarly, the number of segments is determined by the number of this kind of complex solutions, which correspond to the boundary bound states of T^e.

As shown in Fig. 2, different structures of Liouvillian spectrum are characterized by different numbers of segments in four regions. Boundaries of phases with different spectrum structures can be determined by boundaries of parameter regions with different numbers of complex rapidity eigenvalues. To see it clearly, in Fig. 3, we show the change of the odd-parity rapidity spectrum with the parameter h (by fixing $\gamma = 0.2$ and 5, respectively) and γ (by fixing $h = 3$), for the system $N = 100$. In the thermodynamic limit, we can analytically determine the boundaries of regions with different spectrum structures (the details are shown in Appendix B). The odd-parity rapidity spectrum has one pair of pure imaginary eigenvalues in the region with $h < 1$, two pairs of pure imaginary eigenvalues in the region with $h > 1$, $\gamma > 1$ and $h < \frac{1+\gamma^2}{2\gamma}$, no pure imaginary eigenvalue in the region with $h > 1$ and $\gamma < 1$, and two pairs of complex eigenvalues in the region with $h > \frac{1+\gamma^2}{2\gamma}$ and $\gamma > 1$.

As a comparison, we also demonstrate the even-channel rapidity spectrum. To see clearly how the rapidity spectrum changes with parameters, in Fig. 4, we show the change of the even-parity rapidity spectrum with the parameter h (by fixing $\gamma = 0.2$ and 5, respectively) and γ (by fixing $h = 3$), for the system $N = 100$. Compared with the ones from the odd-parity rapidity spectrum in Fig. 3, the real part of the boundary bound states is the same as the ones of the odd-parity rapidity spectrum and the imaginary part of them is only half of the ones of the odd-parity rapidity spectrum. Here the boundary bound states are doubly degenerate. It is shown that the boundaries of different structures of Liouvillian spectrum can be also obtained from the even-channel rapidity spectrum.

IV. LIOUVILLIAN GAP AND RELAXATION DYNAMICS

Next we discuss the Liouvillian gap Δ_g, which is given by the eigenvalue with the largest nonzero real part, i.e., $\Delta_g :=$
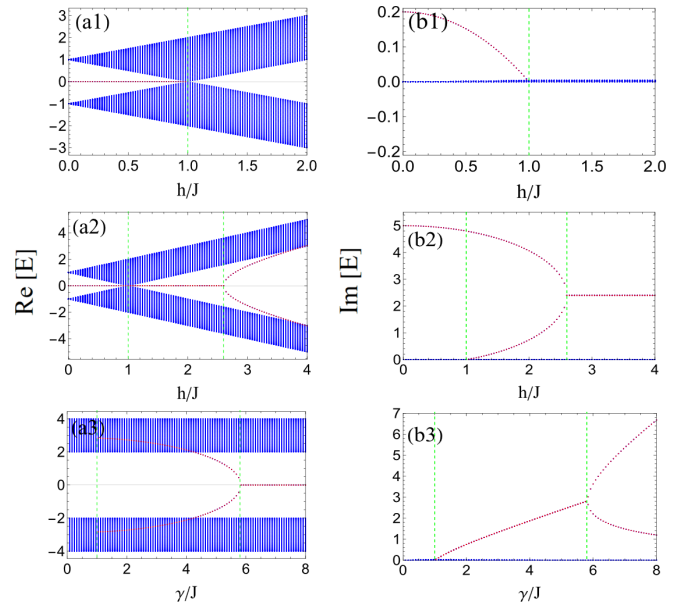

FIG. 4. The rapidity spectrum from the even channel. The red lines denote the nonreal roots corresponding to the boundary bound states and green dash lines indicate the boundaries of regions with different complex solutions. We set the parameters with (a1, b1) $N = 100$, $J = 1$, $\gamma = 0.2$, (a2, b2) $N = 100$, $J = 1$, $\gamma = 5$, and (a3, b3) $N = 100$, $J = 1$, $h = 3$.

$- \max \Re[\lambda]|_{\Re[\lambda]\neq0}$ [15,39]. Explicitly, the Liouvillian gap can be represented as

$$\Delta_g = -\Re\big[2\mathrm{i}\big(E_{j_1,e} + E_{j_2,e}\big)\big], \qquad (24)$$

where $E_{j_1,e}$ and $E_{j_2,e}$ are two eigenvalues with minimum imaginary part in the rapidity spectrum from the even channel. As shown in Figs. 1(b1)–1(b4), the eigenvalues always distribute symmetrically about the imaginary axis, i.e., $E_{j_1,e} = -E^*_{j_2,e}$, due to the K symmetry. We note that the sum of $E_{j_1,e}$ and $E_{j_2,e}$ in Eq. (24) is due to the constraint of parity. If the constraint is not properly accounted, then the Liouvillian gap is underestimated and takes only half of the value of Δ_g.

In the weak and strong dissipation limit, we can derive an analytical expression for the Liouvillian gap by applying a perturbative expansion in terms of the small parameter γ or $1/\gamma$, which leads to

$$\Delta_g \propto \gamma N^{-3}$$

for $\gamma \ll 1$ and

$$\Delta_g \propto \frac{N^{-3}}{\gamma}$$

for $\gamma \gg 1$ (the details are shown in Appendix C). In the thermodynamic limit, we can prove the Liouvillian gap fulfills a dual relation

$$\Delta_g(\gamma, h) = \Delta_g\left(\frac{1}{\gamma}, h\right), \qquad (25)$$

which holds true for arbitrary γ and is irrelevant to h (see Appendix D for the proof). From the dual relation, we can conclude that the Liouvillian gap takes its maximum at $\gamma = 1$ in the whole parameter region of h. As shown in Fig. 5,
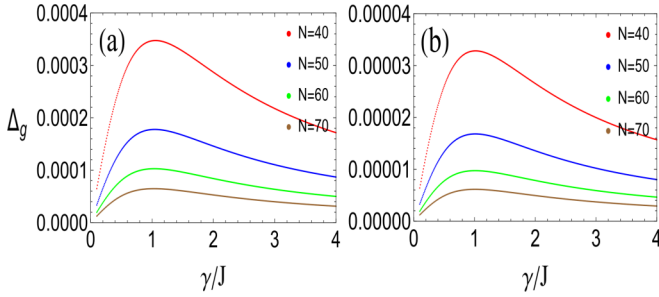
FIG. 5. The Liouvillian gap with (a) $J = 1$, $h = 0.3$ and (b) $J = 1$, $h = 3$.

our numerical results also confirms that the Liouvillian gap increases with the increase of γ in the regime of weak dissipation whereas decreases with the increase of γ in the region of strong dissipation. From the numerical results for system with different sizes, it can be inferred that the inflection point is at $\gamma = 1$ when N tends to infinity, consistent with the duality relation obtained in the thermodynamical limit.

The duality relation of Liouvillian gap also suggests that the relaxation times in the weak ($\gamma \ll 1$) and strong dissipation regions ($\gamma' = 1/\gamma \gg 1$) should be the same. Furthermore, we find that the most of rapidity spectrum satisfies the duality relation $E(\gamma) = E(\frac{1}{\gamma})$ in the thermodynamic limit (see Appendix D), except of those corresponding to the bound states, which contribute to the distance between segments of Liouvillian spectrum. The existence of such a duality relation means that the rightmost segment of Liouvillian spectrum (the one close to the steady state) in the weak ($\gamma \ll 1$) and strong dissipation regions ($\gamma' = 1/\gamma \gg 1$) are almost the same. So we can predict that the system in the weak and strong regions should display almost the same relaxation dynamics when the evolution time enters the region dominated by the rightmost segment, i.e., the existence of a *dynamical duality* in the weak and strong dissipation regions.

To get an intuitive understanding, next we investigate the dynamical behavior by calculating the time-dependent average magnetization denoted as

$$\langle m^z(t) \rangle = \left\langle \frac{1}{N} \sum_{i=1}^{N} \sigma_i^z(t) \right\rangle. \tag{26}$$

The initial state is assumed as $|\rho_0\rangle$ and the vectorizing form of the initial state is $|\rho_0\rangle = \text{vec}(\rho_0)$. Then the time-dependent state can be denoted as $|\rho(t)\rangle = e^{\mathcal{L}t}|\rho_0\rangle$, where the eigen-expansion form of $\mathcal{L}$ is performed as $\mathcal{L} = \sum_i \lambda_i |\psi_i^r\rangle\langle\psi_i^l|$. Then, the average magnetization is rewritten as

$$\langle m^z(t) \rangle = \text{Tr}[m^z(t)\rho(t)] = \langle m^z(t)|\rho(t)\rangle$$
$$= \sum_i e^{\lambda_i t}\langle m^z(t)|\psi_i^r\rangle\langle\psi_i^l|\rho_0\rangle, \tag{27}$$

where $\langle m^z(t)| \equiv [\text{vec}(m^z(t)^\dagger)]^\dagger$. Here, we choose the state with all spin up as the initial state.

Because the Liouvillian of our model is quadratic form, alternatively we can calculate the average magnetization by using Lyapunov equation method [40] (see Appendix E), which enable us to calculate the dynamics of systems with
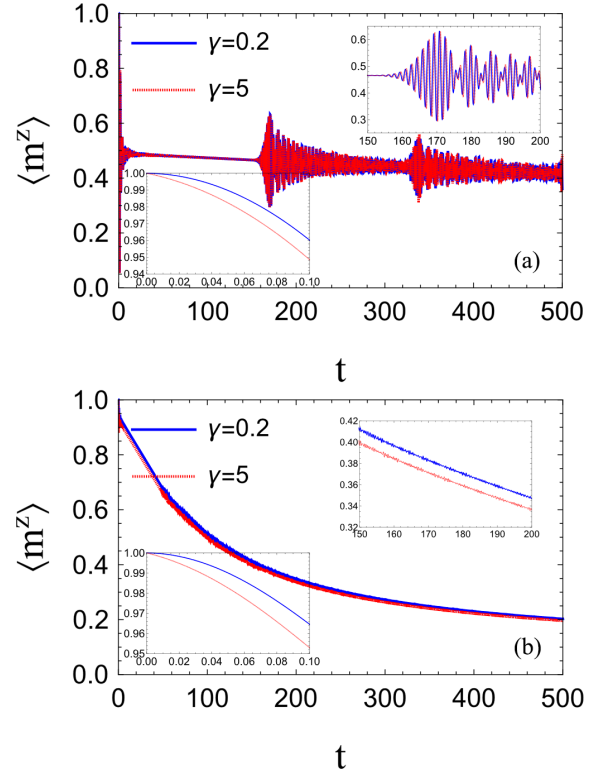

FIG. 6. The dynamical evolution of the average magnetization with $N = 100$, (a) $h = 0.3$ and (b) $h = 3$.

large sizes. We calculate the time-dependent average magnetization in both the weak and strong dissipation regions. By choosing the state with all spin up as the initial state, we display the time evolution of the average magnetization for various parameters in Fig. 6. It is shown that the relaxation dynamics for systems with $\gamma = 0.2$ and 5 are almost identical except in very short time. As the short-time dynamics is mainly determined by the leftmost segment of Liouvillian spectrum, whose center position is determined by the boundary bound state, at the beginning time $\langle m^z(t)\rangle$ decays more slowly for the case with $\gamma = 0.2$ than that with $\gamma = 5$ as shown in the left insets of Fig. 6.

V. SUMMARY

We have exactly solved the transverse field Ising model with boundary dissipations described by the Lindblad master equation. Under a parity constraint, the Liouvillian spectrum is constructed strictly via the rapidity spectrum from both odd and even channels. We find the Liouvillian spectrum displaying four different structures in the whole parameter space and determine the phase boundaries of different structures analytically in the thermodynamical limit. Our analytical results also unveil that the Liouvillian gap fulfills a duality relation in the weak and strong dissipation region and the relaxation dynamics also exhibits a dynamical duality.

Our analytical results unveil that the number of stripes is closely related to the number of complex boundary states in the odd-parity rapidity spectrum. Therefore, we expect that the stripe structures are stable against perturbations. To verify

this, we introduce random onsite disorder perturbation in the transverse field of Hamiltonian (2) and numerically calculate the corresponding Liouvillian spectrum. Our numerical results show that the stripe structures are stable even the perturbed disorder strength is about ten percent of the strength of transverse field. It is also interesting to explore to what extent the dynamical duality exists in other open systems in future works.

APPENDIX A: ANALYTICAL SOLUTION OF THE RAPIDITY SPECTRUM

The full spectrum of Liouvillian $\mathcal{L}$ can be obtained by reorganizing the rapidity spectrum of $\mathcal{L}^P|_{P=1}$ and $\mathcal{L}^P|_{P=-1}$, which can be analytically derived by solving the eigenvalues of the matrix T^P. We consider the general case with $J \neq 0$ and $h \neq 0$ and solve the eigenvalue equation

$$T^P \Psi_P = E_P \Psi_P \tag{A1}$$

by following the analytical method in Ref. [38], where we denote $\Psi_P = (\psi_{1,A}, \psi_{1,B}, \psi_{2,A}, \ldots, \psi_{N,B})^T$.

By substituting Eq. (14) into Eq. (A1), we get a series of bulk equations

$$J\psi_{(n-1),B} + h\psi_{n,B} - E_P\psi_{n,A} = 0,$$
$$h\psi_{(n-1),A} + J\psi_{n,A} - E_P\psi_{(n-1),B} = 0, \tag{A2}$$

with $n = 2, \ldots, N$, and the boundary equations given by

$$P\mathrm{i}\gamma_L\psi_{1,A} + h\psi_{1,B} - E_P\psi_{1,A} = 0,$$
$$h\psi_{N,A} + \mathrm{i}\gamma_R\psi_{N,B} - E_P\psi_{N,B} = 0. \tag{A3}$$

Due to the spatial translational property of bulk equations, we set the ansatz of wave function $|\Psi_P\rangle$ as follows:

$$\Psi_P = (z\phi_A, z\phi_B, z^2\phi_A, z^2\phi_B, \ldots, z^N\phi_A, z^N\phi_B)^T. \tag{A4}$$

By substituting it into the bulk equations Eq. (A2), we obtain

$$Jhz^2 + (J^2 + h^2 - E_P^2)z + Jh = 0. \tag{A5}$$

For a given $E_{j,P}$, there are two solutions $z_i(z_1, z_2)$. According to Vieta's theorem, we can get two constraint equations of them from Eq. (A5):

$$z_1 + z_2 = \frac{E_P^2 - J^2 - h^2}{Jh}, \quad z_1 z_2 = 1. \tag{A6}$$

The constraint condition of Eq. (A6) suggests that the solutions can be represented as

$$z_1 = e^{i\theta}, \quad z_2 = e^{-i\theta}. \tag{A7}$$

In terms of the parameter θ, the eigenvalue can be represented as

$$E_P = \pm\sqrt{J^2 + h^2 + 2Jh\cos\theta}. \tag{A8}$$

The value of θ shall be determined by the boundary equations.

Since the superposition of two linearly independent solutions is also the solution of bulk equations, the general wave function takes the form of

$$\psi_{n,A} = g_1 z_1^n \phi_A^{(1)} + g_2 z_2^n \phi_A^{(2)}, \tag{A9}$$

$$\psi_{n,B} = g_1 z_1^n \phi_B^{(1)} + g_2 z_2^n \phi_B^{(2)}, \tag{A10}$$

where $n = 1, 2, \ldots, N$. To solve the eigenvalue equation (A1), the general ansatz of wave function should also satisfy the boundary conditions. Substituting Eqs. (A9) and (A10) into Eq. (A3), we obtain

$$M_B \begin{pmatrix} g_1 \\ g_2 \end{pmatrix} = \begin{pmatrix} A(z_1, N) & A(z_2, N) \\ B(z_1, N) & B(z_2, N) \end{pmatrix} \begin{pmatrix} g_1 \\ g_2 \end{pmatrix} = 0, \tag{A11}$$

with

$$A(z_i, N) = \frac{P\mathrm{i}\gamma_L}{E_P}(J + hz_i) - J, \tag{A12}$$

$$B(z_i, N) = \frac{\mathrm{i}\gamma_R}{E_P}(h + Jz_i)z_i^N - Jz_i^{N+1}. \tag{A13}$$

The condition for the existence of nontrivial solutions of (g_1, g_2) is determined by $\det[M_B] = 0$ [38,41], which leads to the following equation:

$$p_1 \sin[N\theta] - p_2 \sin[(N+1)\theta] + p_3 \sin[(N-1)\theta] = 0, \tag{A14}$$

where $p_1 = \mathrm{i}J(P\gamma_L + \gamma_R)E_P - (J^3 - JP\gamma_L\gamma_R)$, $p_2 = J^2h$, and $p_3 = hP\gamma_L\gamma_R$. By taking $\gamma_L = \gamma_R = \gamma$, we get Eq. (9) in the main text. If θ is a solution of the above equation, then it is clear that $-\theta$ should be also a solution of the equation. As both θ and $-\theta$ correspond to the same eigenvalue E_P, we can only consider one of them. Then, we can rewrite Eq. (A14) in even channel ($P = 1$) and odd channel ($P = -1$) as

$$[2\mathrm{i}\gamma E_e - (1 - \gamma^2)] \sin[N\theta] - h \sin[(N+1)\theta]$$
$$+ h\gamma^2 \sin[(N-1)\theta] = 0 \tag{A15}$$

and

$$(1 + \gamma^2) \sin[N\theta] + h \sin[(N+1)\theta] + h\gamma^2 \sin[(N-1)\theta] = 0, \tag{A16}$$

respectively.

We note T^P fulfills K symmetry, i.e.,

$$\eta^{-1} T^P \eta = -(T^P)^*, \tag{A17}$$

where η is a diagonal matrix with the elements $[-1, 1, -1, \ldots, (-1)^{2N}]$. The existence of K symmetry implies that if E is an eigenvalue of T^P, then $-E^*$ is also an eigenvalue of T^P, i.e., both the even-parity and odd-parity rapidity spectra should distribute symmetrically about the imaginary axis. For convenience, we shall use T^e and T^o to denote T^P with $P = 1$ (even parity) and $P = -1$ (odd parity), respectively.
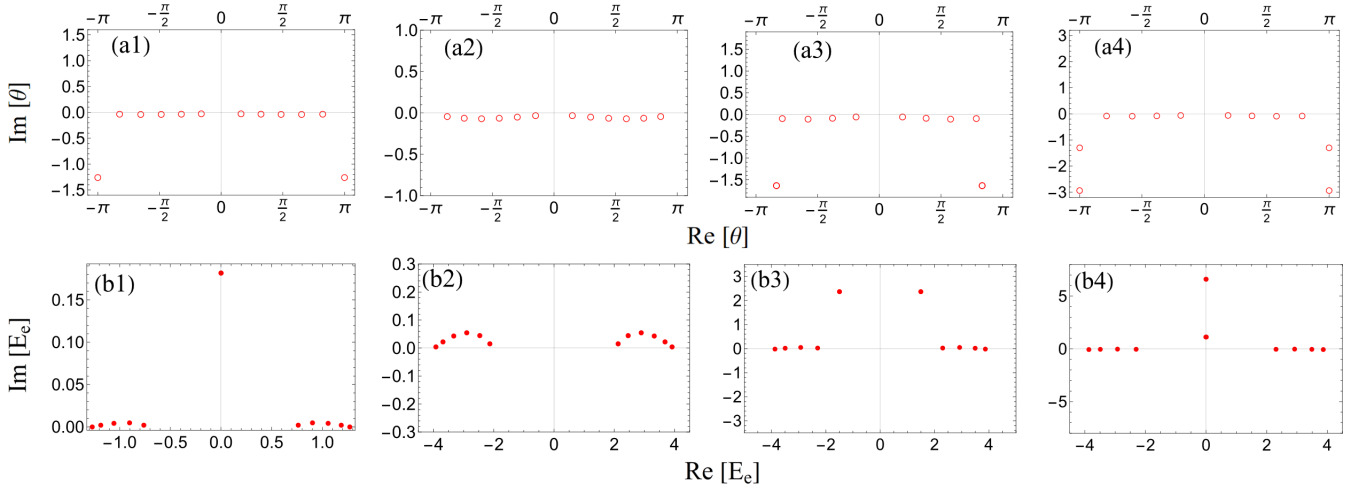
FIG. 7. The solutions of Eq. (21) and the rapidity spectrum with $N = 6$, (a1, b1) $J = 1$, $h = 0.3$, $\gamma = 0.2$, (a2, b2) $J = 1$, $h = 3$, $\gamma = 0.2$, (a3, b3) $J = 1$, $h = 3$, $\gamma = 5$, and (a4, b4) $J = 1$, $h = 3$, $\gamma = 8$. The red empty circles represent the solutions of Eq. (21), while the red points represent the rapidity spectrum from the even-parity channel.

For the even parity ($P = 1$), T^e is invariant under the reflection operation, i.e.,

$$\mathscr{P} T^e \mathscr{P} = T^e. \tag{A18}$$

For the odd parity ($P = -1$), T^o fulfills the $\mathscr{P}\mathscr{T}$ symmetry, i.e.,

$$[\mathscr{P}\mathscr{T}, T^o] = 0. \tag{A19}$$

The existence of $\mathscr{P}\mathscr{T}$ symmetry suggests that the eigenvalues of T^o are either real or distribute symmetrically about the real axis, i.e., if E is an eigenvalue of T^o, then E^* is also an eigenvalue of T^o.

For convenience, we denote the eigenvalues as $E_\pm(\theta) = \pm\sqrt{J^2 + h^2 + 2Jh\cos\theta}$, with $\Re[\sqrt{J^2 + h^2 + 2Jh\cos\theta}] > 0$. While the solutions of θ are always complex for the even-parity case, they can be real or complex for the odd-parity case. According to the expression of $E_\pm(\theta)$, we have $E_\pm(\theta)^* = E_\pm(\theta^*)$. If we assume that $E_+(\theta)$ is an eigenvalue of T^e, then we can get $E_-(\theta^*)$ is also the eigenvalue of T^e, i.e., when θ satisfies the Eq. (A15) with $E_e = E_+$, then θ^* satisfies the Eq. (A15) with $E_e = E_-$. According to Eq. (A15), we can see that $-\theta^*$ is also the solution of Eq. (A15) and $E_-(-\theta^*) = E_-(\theta^*)$. In the odd-parity channel, the matrix T^o has $\mathscr{P}\mathscr{T}$ symmetry and K symmetry. We can get that when $E_+(\theta)$ is an eigenvalue of T^o, then $E_+(\theta^*)$, $E_-(\theta)$, $E_-(\theta^*)$ are also the eigenvalues of T^o. So, when θ satisfies Eq. (A16), then θ^* also satisfies Eq. (A16).

To see clearly how the solutions of θ are related to the rapidity spectrum, in Figs. 7 and 8 we demonstrate the solutions of Eqs. (A15) and (A16), respectively, and the corresponding even-parity and odd-parity rapidity spectrum for the four typical cases in Fig. 1. In Fig. 7, the solutions satisfying with $\Re[\theta] > 0$ correspond to E_+ and the solutions satisfying with $\Re[\theta] < 0$ correspond to E_-. In Fig. 7(a3), we note that the solutions of θ given by $2.61894 - 1.60997i$ and $2.61962 - 1.60891i$ are nearly degenerate. Similarly, the solutions given by $-2.61894 - 1.60997i$ and $-2.61962 - 1.60891i$ are nearly degenerate. These solutions become exactly degenerate in the thermodynamical limit $N \to \infty$.

APPENDIX B: DETERMINE THE BOUNDARY OF THE SCHEMATIC PHASE DIAGRAM

In the limit of $N \to \infty$, we can determine the boundary of schematic phase diagram by analyzing the solutions of Eq. (22) and the odd-parity rapidity spectrum. We note that, in three-segment and nine-segment regions of the schematic phase diagram, the odd-parity rapidity spectrum has one pair and two pairs of pure imaginary eigenvalues, respectively. Next we look for conditions for the existence of pure imaginary rapidity eigenvalues. Without loss of generality, we assume the solution of Eq. (22) as $\theta = \theta_R + i\theta_I$ and θ_R, θ_I are purely real. Then, we can rewrite the corresponding eigenvalue as

$$E_o = \pm\sqrt{1 + h^2 + 2h\cos[\theta_R + i\theta_I]}. \tag{B1}$$

If the eigenvalue E_o is pure imaginary, then we should have $\theta_R = \pi$, and thus the eigenvalue can be expressed as

$$E_o = \pm\sqrt{1 + h^2 - 2h\cosh[\theta_I]}. \tag{B2}$$

Substituting $\theta = \pi + i\theta_I$ into Eq. (22), we can get

$$f_1 \sinh[N\theta_I] - f_2 \sinh[(N+1)\theta_I]$$
$$- f_3 \sinh[(N-1)\theta_I] = 0, \tag{B3}$$

where $f_1 = (1 + \gamma^2)$, $f_2 = h$, $f_3 = h\gamma^2$. In the thermodynamic limit of $N \to \infty$, we can use the formula

$$2\sinh[N\theta_I] \approx \text{sign}[\theta_I] e^{N|\theta_I|}, \tag{B4}$$

and thus Eq. (B3) is simplified to

$$f_1 e^{N|\theta_I|} - f_2 e^{(N+1)|\theta_I|} - f_3 e^{(N-1)|\theta_I|} = 0, \tag{B5}$$

which gives rise to

$$f_1 e^{|\theta_I|} - f_2 e^{2|\theta_I|} - f_3 = 0. \tag{B6}$$

Let $x = e^{|\theta_I|}$, and the solutions of x are given by

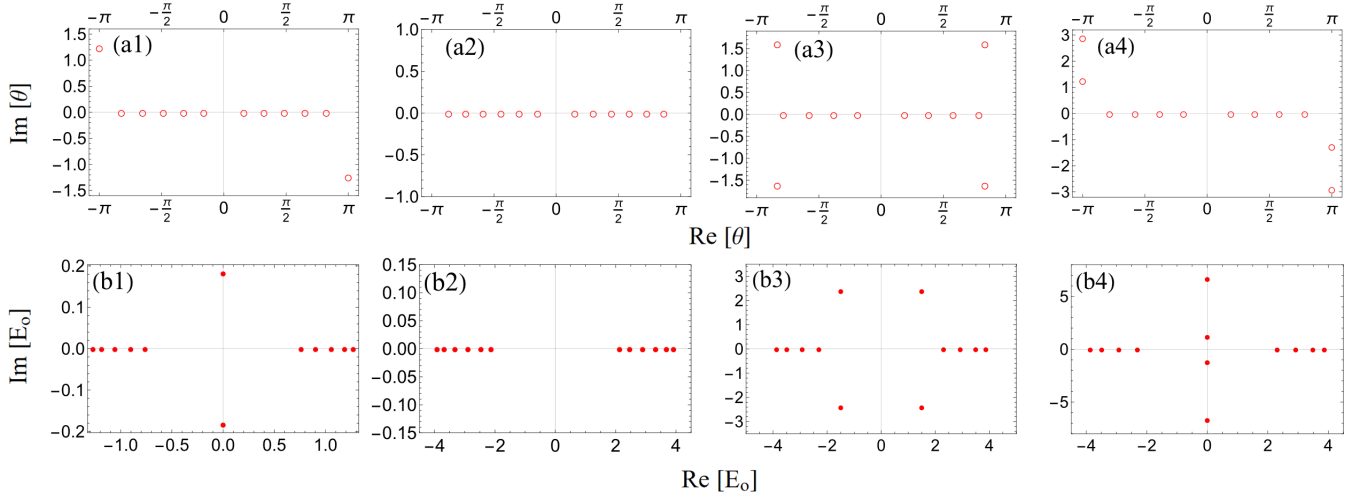$$x = \frac{1 + \gamma^2 \pm \sqrt{(1 + \gamma^2)^2 - 4h^2\gamma^2}}{2h}. \tag{B7}$$

FIG. 8. The solutions of Eq. (22) and the rapidity spectrum with $N = 6$, (a1, b1) $J = 1$, $h = 0.3$, $\gamma = 0.2$, (a2, b2) $J = 1$, $h = 3$, $\gamma = 0.2$, (a3, b3) $J = 1$, $h = 3$, $\gamma = 5$, and (a4, b4) $J = 1$, $h = 3$, $\gamma = 8$. The red empty circles represent the solutions of Eq. (22), while the red points represent the rapidity spectrum from the odd-parity channel.

For convenience, we denote the above two solutions as $x_{\pm} = e^{|\theta_I(\pm)|}$. For any nonzero solution of θ_I, we always have $x > 1$. If $x_{\pm} > 1$, then we have two solutions $\theta_I(\pm)$, corresponding to two pairs of pure imaginary eigenvalues. If only one of $x_{\pm}$ is larger than 1, then we have one pair of pure imaginary eigenvalues. If $x_{\pm} < 1$, then no pure imaginary eigenvalue exits.

Next, we discuss in detail and set $h > 0$, $\gamma > 0$. When $x_{\pm} > 1$, we get the constraint equations as follows:

$$(1 + \gamma^2)^2 - 4h^2\gamma^2 \geqslant 0,$$

$$\times 1 + \gamma^2 + \sqrt{(1 + \gamma^2)^2 - 4h^2\gamma^2}2h > 1,$$

$$\times \frac{1 + \gamma^2 - \sqrt{(1 + \gamma^2)^2 - 4h^2\gamma^2}}{2h} > 1. \quad (B8)$$

Thus, we can get the boundary of nine-segment phase is $1 < \gamma$ and $1 < h \leqslant \frac{1+\gamma^2}{2\gamma}$.

For the three-segment phase, only one of $x_{\pm}$ is larger than 1, and the constraint equations are as follows:

$$(1 + \gamma^2)^2 - 4h^2\gamma^2 \geqslant 0,$$

$$\times \frac{1 + \gamma^2 + \sqrt{(1 + \gamma^2)^2 - 4h^2\gamma^2}}{2h} > 1,$$

$$\times \frac{1 + \gamma^2 - \sqrt{(1 + \gamma^2)^2 - 4h^2\gamma^2}}{2h} \leqslant 1. \quad (B9)$$

Here, it is easy to certify $x_+ \geqslant x_-$. Then we can get the boundary of three-segment phase is $0 < h < 1$ (or $h = 1$ and $\gamma > 1$).

When $\gamma = 1$, Eq. (22) reduces to

$$-2\sin[N\theta] - h\sin[(N+1)\theta] - h\sin[(N-1)\theta] = 0, \quad (B10)$$

which leads to

$$\sin[N\theta](1 + h\cos[\theta]) = 0. \quad (B11)$$

From the above equation, we see that the solutions are determined by

$$\sin[N\theta] = 0, \quad 1 + h\cos[\theta] = 0, \quad (B12)$$

which give rise to $\theta = \frac{j\pi}{N}, (j = 1, \ldots, N)$ and $\theta = \arccos[-\frac{1}{h}]$. Here, $\theta = \pi$ should be abandoned, because $\theta = \pi$ corresponds to $z_1 = z_2$ and thus Eqs. (A9) and (A10) are not linearly independent. When $h < 1$, the equation $1 + h\cos[\theta] = 0$ has no purely real solution, and the solution is given by $\theta = \pi + i\theta_I$ with $\theta_I = \text{arcosh}[1/h]$, corresponding to the existence of one pair of imaginary eigenvalues in the rapidity spectrum. When $h > 1$, $\theta = \arccos[-\frac{1}{h}]$ is purely real and the odd-parity rapidity spectrum is purely real. The line of $\gamma = 1$ and $h > 1$ is the phase boundary between the five-segment and one-segment regions. In the region of $h > 1$ and $\gamma < 1$, all solutions of Eq. (22) are real.

Next we analyze the boundary bound states of the even-channel rapidity spectrum in the thermodynamic limit of $N \to \infty$. In Figs. 4(a2) and 4(b2), it is shown that the even-parity rapidity spectrum has one degenerate imaginary eigenvalue and two degenerate imaginary eigenvalues in three-segment and nine-segment regions of the schematic phase diagram, respectively. So, we assume the solution of Eq. (21) as $\theta = \theta_R + i\theta_I$ and θ_R, θ_I are purely real. Then, we can rewrite the corresponding eigenvalue as

$$E_e = \pm\sqrt{1 + h^2 + 2h\cos[\theta_R + i\theta_I]}. \quad (B13)$$

If the eigenvalue E_e is pure imaginary, then we should have $\theta_R = \pi$, and thus the eigenvalue can be expressed as

$$E_e = \pm\sqrt{1 + h^2 - 2h\cosh[\theta_I]}. \quad (B14)$$

Substituting $\theta = \pi + i\theta_I$ into Eq. (21), we can get

$$4\gamma^2 E_e^2 \sinh[N\theta_I]^2 + [(2 - f_1)\sinh[N\theta_I]$$
$$- f_2\sinh[(N+1)\theta_I] + f_3\sinh[(N-1)\theta_I]]^2 = 0, \quad (B15)$$

where $f_1 = (1 + \gamma^2)$, $f_2 = h$, $f_3 = h\gamma^2$. In the thermodynamic limit of $N \to \infty$, we can use the formula

$$2 \sinh [N\theta_I] \approx \text{sign}[\theta_I] e^{N|\theta_I|}, \tag{B16}$$

and thus the Eq. (B15) is simplified to

$$\left(f_1 e^{N|\theta_I|} - f_2 e^{(N+1)|\theta_I|} - f_3 e^{(N-1)|\theta_I|}\right)^2 = 0, \tag{B17}$$

which gives rise to

$$f_1 e^{|\theta_I|} - f_2 e^{2|\theta_I|} - f_3 = 0. \tag{B18}$$

Let $x = e^{|\theta_I|}$, and the solutions of x are given by

$$x = \frac{1 + \gamma^2 \pm \sqrt{(1 + \gamma^2)^2 - 4h^2\gamma^2}}{2h}. \tag{B19}$$

It is easy to see that the results are the same as the analysis about Eq. (B7).

APPENDIX C: SCALING RELATION OF LIOUVILLIAN GAP

For the case of $\gamma_L = \gamma_R = \gamma$, the Liouvillian gap comes from even channel, i.e., determined by the solutions of

$$(\gamma^2 - 1 + 2iE_e\gamma)\sin[N\theta] + h\gamma^2 \sin[(N-1)\theta] \\ - h\sin[(N+1)\theta] = 0. \tag{C1}$$

In general, solutions of the above equation are always complex. In the limits of weak and strong dissipation, we can derive analytical expression of Liouvillian gap by applying perturbation theory.

First, we consider the weak dissipation limit with $\gamma \ll 1$ and $E_e = \sqrt{1 + h^2 + 2h\cos[\theta]}$. By taking γ as a small parameter for the perturbation calculation, the zero-order solution of θ is determined by

$$\sin\left[N\theta^{(0)}\right] + h\sin\left[(N+1)\theta^{(0)}\right] = 0. \tag{C2}$$

Thus, we can get

$$\theta_j^{(0)} \simeq \begin{cases} \frac{j\pi}{N} - \frac{h}{N}\sin\left[\frac{j\pi}{N}\right] & \left(h \ll \frac{1}{N}\right), \\ \frac{2j\pi}{2N+1} & (h = 1), \\ \frac{j\pi}{N+1} + \frac{1}{h(N+1)}\sin\left[\frac{j\pi}{N+1}\right] & \left(\frac{1}{h} \ll \frac{1}{N}\right), \end{cases} \tag{C3}$$

where $j = 1, 2, \ldots, N$. Then we use the perturbation theory and assume $\theta_j = \theta_j^{(0)} + \gamma\theta_j^{(1)}$ with $\gamma \ll 1$. Substituting it into Eq. (C1), we can get

$$\theta_j^{(1)} = -\frac{h\sin\left[(N+1)\theta_j^{(0)}\right] + \sin\left[N\theta_j^{(0)}\right]}{\left(h(N+1)\cos\left[(N+1)\theta_j^{(0)}\right] + N\cos\left[N\theta_j^{(0)}\right]\right)}\gamma \\ + i\frac{2E_{j,1}^{(0)}\sin\left[N\theta_j^{(0)}\right]}{h(N+1)\cos\left[(N+1)\theta_j^{(0)}\right] + N\cos\left[N\theta_j^{(0)}\right]}, \tag{C4}$$

where $E_e^{(0)} = \sqrt{1 + h^2 + 2h\cos[\theta_j^{(0)}]}$. Thus, to the first order

of γ, the spectrum can be approximately written as

$$E_e \approx E_e^{(0)}\sqrt{1 - \frac{2h\gamma\theta_j^{(1)}\sin\left[\theta_j^{(0)}\right]}{\left(E_e^{(0)}\right)^2}}$$

$$\approx E_e^{(0)}\left(1 - \frac{h\gamma\theta_j^{(1)}\sin\theta_j^{(0)}}{\left(E_e^0\right)^2}\right)$$

$$= E_e^{(0)} - \frac{h\theta_j^{(1)}\sin\theta_j^{(0)}}{E_e^{(0)}}\gamma, \tag{C5}$$

and the imaginary part of rapidity spectrum from the even channel can be written as

$$I_j \simeq \left|\frac{2\gamma h\sin\left[\theta_j^{(0)}\right]\sin\left[N\theta_j^{(0)}\right]}{h(N+1)\cos\left[(N+1)\theta_j^{(0)}\right] + N\cos\left[N\theta_j^{(0)}\right]}\right|. \tag{C6}$$

We find that I_j with $j = 1$ is the minimum, which is the same as the numerical result. So, we set $\theta^{(0)} = \theta_1^{(0)}$. Thus, the Liouvillian gap is given by

$$\Delta_g = 4I_1$$

$$= \left|\frac{8\gamma h\sin\left[\theta^{(0)}\right]\sin\left[N\theta^{(0)}\right]}{h(N+1)\cos\left[(N+1)\theta^{(0)}\right] + N\cos\left[N\theta^{(0)}\right]}\right|. \tag{C7}$$

It follows that the scaling of the Liouvillian gap with lattice size N is given by

$$\Delta_g \propto \gamma N^{-3}, \tag{C8}$$

where $\sin[\theta^{(0)}] \propto N^{-1}$, $\sin[N\theta^{(0)}] \propto N^{-1}$, $\cos[N\theta^{(0)}] \propto N^0$ in the thermodynamic limit.

Now we consider the strong dissipation limit with $\gamma \gg 1$. We can rewrite Eq. (C1) as

$$\left(1 - \frac{1}{\gamma^2} + \frac{2iE_e}{\gamma}\right)\sin[N\theta] + h\sin[(N-1)\theta] \\ - \frac{h}{\gamma^2}\sin[(N+1)\theta] = 0. \tag{C9}$$

For $\gamma \gg 1$ and $E_e = \sqrt{1 + h^2 + 2h\cos[\theta^{(0)}]}$, we can take $1/\gamma$ as a small parameter for perturbation calculation, and the zero-order solution of θ_j is determined by

$$\sin\left[N\theta^{(0)}\right] + h\sin\left[(N-1)\theta^{(0)}\right] = 0. \tag{C10}$$

Thus, we can get

$$\theta_j^{(0)} \simeq \begin{cases} \frac{j\pi}{N} + \frac{h}{N}\sin\left[\frac{j\pi}{N}\right] & \left(h \ll \frac{1}{N}\right), \\ \frac{2j\pi}{2N-1} & (h = 1), \\ \frac{j\pi}{N-1} - \frac{1}{h(N-1)}\sin\left[\frac{j\pi}{N-1}\right] & \left(\frac{1}{h} \ll \frac{1}{N}\right), \end{cases} \tag{C11}$$

where $j = 1, 2, \ldots, N$. Then we use the perturbation theory and assume $\theta_j = \theta_j^{(0)} + \frac{1}{\gamma}\theta_j^{(1)}$ with $\gamma \gg 1$. Substituting it into Eq. (C9), we can get

$$\theta_j^{(1)} = -\frac{\left(h\sin\left[(N+1)\theta_j^{(0)}\right] + \sin\left[N\theta_j^{(0)}\right]\right)\gamma}{h(N-1)\cos\left[(N-1)\theta_j^{(0)}\right] + N\cos\left[N\theta_j^{(0)}\right]} \\ - i\frac{2E_{j,1}^{(0)}\sin\left[N\theta_j^{(0)}\right]}{h(N-1)\cos\left[(N-1)\theta_j^{(0)}\right] + N\cos\left[N\theta_j^{(0)}\right]}, \tag{C12}$$

where $E_e^{(0)} = \sqrt{1 + h^2 + 2h\cos[\theta_j^{(0)}]}$.

Thus, to the order of $1/\gamma$, the spectrum can be approximately represented as

$$
\begin{aligned}
E_e &\approx E_e^0 \sqrt{1 - \frac{2h\theta_j^{(1)}\sin\left[\theta_j^{(0)}\right]}{\gamma\left(E_e^{(0)}\right)^2}} \\
&\approx E_e^0\left(1 - \frac{h\gamma\theta_j^{(1)}\sin\theta_j^{(0)}}{\gamma\left(E_e^0\right)^2}\right) \\
&= E_e^{(0)} - \frac{h\theta_j^{(1)}\sin\theta_j^{(0)}}{E_e^{(0)}\gamma},
\end{aligned}
\tag{C13}
$$

and the imaginary part of rapidity spectrum from the even channel can be written as

$$
\mathrm{I}_j \simeq \left| \frac{2h\sin\left[\theta_j^{(0)}\right]\sin\left[N\theta_j^{(0)}\right]}{\left(h(N-1)\cos\left[(N-1)\theta_j^{(0)}\right] + N\cos\left[N\theta_j^{(0)}\right]\right)\gamma} \right|.
\tag{C14}
$$

We find that I_j with $j = 1$ is the minimum, which is the same as the numerical result. So, we set $\theta^{(0)} = \theta_1^{(0)}$. Thus, the Liouvillian gap is given by

$$
\begin{aligned}
\Delta_g &= 4\mathrm{I}_1 \\
&= \left| \frac{8h\sin\left[\theta^{(0)}\right]\sin\left[N\theta^{(0)}\right]}{\left(h(N-1)\cos\left[(N-1)\theta^{(0)}\right] + N\cos\left[N\theta^{(0)}\right]\right)\gamma} \right|.
\end{aligned}
\tag{C15}
$$

It follows that the scaling of the Liouvillian gap with lattice size N is given by

$$
\Delta_g \propto \frac{N^{-3}}{\gamma},
\tag{C16}
$$

where $\sin[\theta_j^{(0)}] \propto N^{-1}$, $\sin[N\theta_j^{(0)}] \propto N^{-1}$, $\cos[N\theta_j^{(0)}] \propto N^0$ in the thermodynamic limit. We note that if we choose $E_e = -\sqrt{1 + h^2 + 2h\cos[\theta^{(0)}]}$, we get the same result of Liouvillian gap.

APPENDIX D: DUALITY RELATION OF RAPIDITY SPECTRUM AND LIOUVILLIAN GAP IN THE THERMODYNAMIC LIMIT

The rapidity spectrum of the even-parity channel is determined by solving the following equation:

$$
\begin{aligned}
(\gamma^2 - 1 + 2i\gamma E_e)\sin[N\theta] + h\gamma^2 \sin[(N-1)\theta] \\
- h\sin[(N+1)\theta] = 0,
\end{aligned}
\tag{D1}
$$

where $E_e = \pm\sqrt{1 + h^2 + 2h\cos[\theta]}$. Here, we should notice the solutions corresponding to two equations ($E_\pm(\theta_\pm) = \pm\sqrt{1 + h^2 + 2h\cos[\theta_\pm]}$) and denote the solutions of them as $\theta_\pm$, respectively, i.e.,

$$
\sin[N\theta_\pm] + h\gamma^2 \sin[(N-1)\theta_\pm] - h\sin[(N+1)\theta_\pm] = 0,
\tag{D2}
$$

where $E_\pm(\theta_\pm) = \pm\sqrt{1 + h^2 + 2h\cos[\theta_\pm]}$. According to Eq. (D2), if θ_+ is a solution of the equation with eigenvalue $E_+(\theta_+)$, then θ_+^* should be a solution of

the equation with eigenvalue $E_-(\theta_-)$, i.e., we have $\theta_-(\lambda) = \theta_+^*(\lambda)$. Similarly, we can prove $\theta_+(\lambda) = \theta_-^*(\lambda)$. So we have $E_-(\theta_-) = E_-(\theta_+^*) = -E_+(\theta_+^*) = -(E_+(\theta_+))^*$ and $E_+(\theta_+) = -E_-(\theta_-^*) = -(E_-(\theta_-))^*$, which are consistent with the requirement of the K symmetry.

First, we consider the case of E_+ and get the equation as follows:

$$
\sin[N\theta_+] + h\gamma^2 \sin[(N-1)\theta_+] - h\sin[(N+1)\theta_+] = 0.
\tag{D3}
$$

Then we consider the equation of E_- with the dissipation strength γ', and Eq. (D2) can be rewritten as

$$
\begin{aligned}
(\gamma'^2 - 1 + 2i\gamma' E_-(\theta_-))\sin[N\theta_-] + h\gamma'^2 \sin[(N-1)\theta_-] \\
- h\sin[(N+1)\theta_-] = 0.
\end{aligned}
\tag{D4}
$$

By using the relation $E_-(\theta_-) = -(E_+(\theta_+))^* = -E_+(\theta_+^*)$ and $\theta_- = \theta_+^*$, Eq. (D4) can be rewritten as

$$
\begin{aligned}
(\gamma'^2 - 1 - 2i\gamma' E_+(\theta_+^*))\sin[N\theta_+^*] + h\gamma'^2 \sin[(N-1)\theta_+^*] \\
- h\sin[(N+1)\theta_+^*] = 0.
\end{aligned}
\tag{D5}
$$

Now we assume $\gamma' = \frac{1}{\gamma}$ and thus the above equation can be represented as follows:

$$
\begin{aligned}
(\gamma^2 - 1 + 2i\gamma E_+(\theta_+^*))\sin[N\theta_+^*] + h\gamma^2 \sin[(N+1)\theta_+^*] \\
- h\sin[(N-1)\theta_+^*] = 0.
\end{aligned}
\tag{D6}
$$

When the real part of θ_+ is proportional to $\frac{1}{N}$ and the imaginary part of θ_+ is proportional to $\frac{1}{N^2}$, we have $\sin[(N-1)\theta_+] \approx \sin[(N+1)\theta_+]$ in the thermodynamic limit. Comparing Eqs. (D3) and (D6), we can consider them to be the same in the thermodynamic limit. Since Eqs. (D4) and (D6) are equivalent, then we get $\theta_+(\gamma) \approx \theta_-^*(\frac{1}{\gamma})$ in the thermodynamic limit. Using the relation $\theta_-^*(\frac{1}{\gamma}) = \theta_+(\frac{1}{\gamma})$, we can get $\theta_+(\gamma) \approx \theta_+(\frac{1}{\gamma})$. According to the above analysis, we have $E_+(\gamma) = E_+(\frac{1}{\gamma})$ in the thermodynamic limit. Similarly, we can get $E_-(\gamma) = E_-(\frac{1}{\gamma})$ in the thermodynamic limit. So, we can get

$$
E_e(\gamma) = E_e\left(\frac{1}{\gamma}\right)
\tag{D7}
$$

in the thermodynamic limit. Notice that for the boundary bound states, the real parts of them are not proportional to $\frac{\pi}{N}$ and thus the approximation $\sin[(N-1)\theta_+] \approx \sin[(N+1)\theta_+]$ does not hold true.

According to the definition of Liouvillian gap, it follows that the Liouvillian gap fulfills

$$
\Delta_g(\gamma, h) = \Delta_g\left(\frac{1}{\gamma}, h\right).
\tag{D8}
$$

We have proven that the most of rapidity spectrum (except for those corresponding to the boundary bound states) satisfies the duality relation $E(\gamma) = E(\frac{1}{\gamma})$ in the thermodynamic limit. The eigenvalues of boundary bound states do not satisfy the duality relation, e.g., the imaginary part of the boundary bound state (the one with larger imaginary part) increases
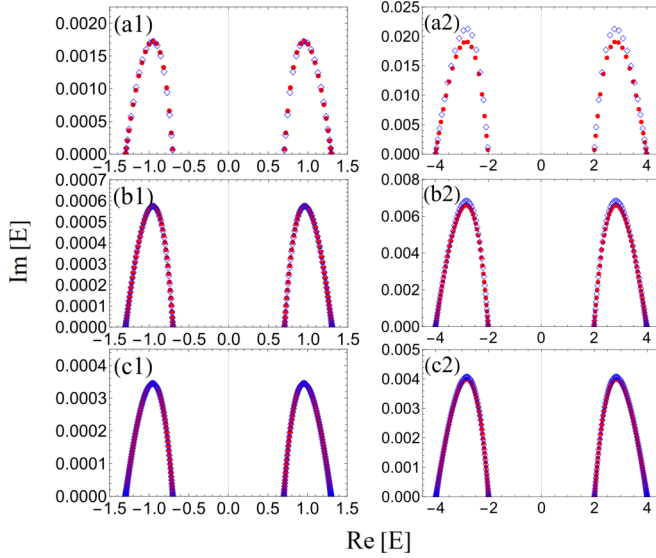
FIG. 9. The rapidity spectrum from even channels (except for eigenvalues corresponding to the boundary bound states) with $N = 20$, (a1) $h = 0.3$, and (a2) $h = 3$, and $N = 60$, (b1) $h = 0.3$, and (b2) $h = 3$, and $N = 100$, (c1) $h = 0.3$, and (c2) $h = 3$. We take parameter $\gamma = 0.2$ which corresponds to the red points and $\gamma = 5$ which corresponds to the blue empty prismatic.

with the increase of γ as displayed in Fig. 4(b3). In Fig. 9, we show the rapidity spectrum of the even channel except for the boundary bound state. While the number of bound states in the weak and strong dissipation regions are the same in the region of $h < 1$, they are different in the region of $h > 1$. This leads to the spectrum $E(\gamma)$ and $E(1/\gamma)$ in the region of $h = 0.3$ coinciding much better than in the region of $h = 3$, as shown in Figs. 9(a1) and 9(a2) for $N = 20$. With the increase of lattice size, the spectrum $E(\gamma)$ and $E(1/\gamma)$ coincide much better. While the spectrum $E(\gamma)$ and $E(1/\gamma)$ do not coincide very well for the case of $h = 3$ with $N = 20$, they are almost the same with $N = 100$.

APPENDIX E: CALCULATION OF THE AVERAGE MAGNETIZATION BY USING LYAPUNOV EQUATION METHOD

Here we show the details of calculation of the average magnetization by using Lyapunov equation method [40]. Lyapunov equation method enables us to calculate the dynamics of systems with large sizes. In terms of the representation of Majorana fermion, we can rewrite the transverse field Ising chain and the dissipation operators as $\hat{H} = \sum_{i,j} \hat{w}_i H_{i,j} \hat{w}_j$, $\hat{L}_\mu = \sum_j l_{\mu,j} \hat{w}_j$. The matrix Γ is also defined as Majorana fermion $\Gamma_{j,k} = i\langle \hat{w}_j \hat{w}_k \rangle - \frac{i}{2}\delta_{j,k}$. And then we have

$$\partial_t \Gamma = X\Gamma + \Gamma X^T + Y, \tag{E1}$$

where the matrix X, Y are defined as $X = -2iH - \Re(\sum_\mu l_\mu l_\mu^\dagger)$, $Y = \Im(\sum_\mu l_\mu l_\mu^\dagger)$, respectively. And l_μ can be expressed as $l_\mu = [l_{\mu,1}, l_{\mu,2}, \ldots l_{\mu,2N}]^T$.

First, we apply the Jordan-Wigner transformation

$$\hat{a}_j^\dagger = \frac{1}{2}\left(\sigma_j^x + i\sigma_j^y\right)\prod_{l=1}^{j-1}\left(\sigma_l^z\right) \quad (1 \leqslant j \leqslant N). \tag{E2}$$

Here, $\hat{a}_j$ and $\hat{a}_j^\dagger$ obey the canonical anticommutation relations $\{\hat{a}_i, \hat{a}_j^\dagger\} \equiv \hat{a}_i\hat{a}_j^\dagger + \hat{a}_j^\dagger\hat{a}_i = \delta_{i,j}$ and $\{\hat{a}_i, \hat{a}_j\} = \{\hat{a}_i^\dagger, \hat{a}_j^\dagger\} = 0$. And then, the transverse field Ising chain can be written as fermion form

$$H = J\sum_{j=1}^{N-1}(\hat{a}_j^\dagger - \hat{a}_j)(\hat{a}_{j+1}^\dagger + \hat{a}_{j+1}) - h\sum_{j=1}^{N}(\hat{a}_j^\dagger - \hat{a}_j)(\hat{a}_j^\dagger + \hat{a}_j). \tag{E3}$$

Then, we employ the self-adjoint Majorana operators $\hat{w}_{j,\pm} = (\hat{w}_{j,\pm})^\dagger$ [40],

$$\begin{pmatrix} \hat{w}_{j,+} \\ \hat{w}_{j,-} \end{pmatrix} := \frac{1}{\sqrt{2}}\begin{pmatrix} 1 & 1 \\ i & -i \end{pmatrix}\begin{pmatrix} \hat{a}_j \\ \hat{a}_j^\dagger \end{pmatrix}, \tag{E4}$$

and we get

$$\hat{H} = 2i\left(J\sum_{j=1}^{N-1}\hat{w}_{j,-}\hat{w}_{j+1,+} + h\sum_{j=1}^{N}\hat{w}_{j,+}\hat{w}_{j,-}\right). \tag{E5}$$

For convenience, we denote

$$\hat{w}_j := \hat{w}_{j,+} \quad \text{and} \quad \hat{w}_{j+N} := \hat{w}_{j,-}. \tag{E6}$$

The Majorana operators with $j = 1, \ldots, N$. They obey the anticommutation relations

$$\{\hat{w}_i, \hat{w}_j\} = \delta_{i,j} \quad \text{for} \quad i, j = 1, \ldots, 2N. \tag{E7}$$

Thus, we get the transverse field Ising chain as

$$\hat{H} = \sum_{i,j} \hat{w}_i H_{i,j} \hat{w}_j. \tag{E8}$$

And the boundary dissipation operators can be rewritten as

$$\hat{L}_L = \sqrt{2\gamma}\hat{w}_{1,+}, \hat{L}_R = iQ\sqrt{2\gamma}\hat{w}_{N,-}, \tag{E9}$$

where $Q = \prod_{j=1}^{N}\sigma_j^z$ is the parity operator. In our case, the initial state is the even fermion state and the operator m^z is also even fermion. Thus, the distribution of the odd channel is zero, so we can only consider the average magnetization in the even channel, i.e., $Q = 1$. Thus, the matrix X, Y is represented in terms of a $2N \times 2N$ non-Hermitian matrix as follows:

$$X = \begin{bmatrix} -2\gamma & & & & 2h & & & \\ & 0 & & & -2J & \ddots & & \\ & & \ddots & & & \ddots & \ddots & \\ & & & 0 & & & -2J & 2h \\ -2h & 2J & & & 0 & & & \\ \ddots & \ddots & & & & \ddots & & \\ & \ddots & 2J & & & & 0 & \\ & & -2h & & & & & -2\gamma \end{bmatrix},$$

$$Y = 0_{2N}. \tag{E10}$$

And then we give the spectral representation of X,

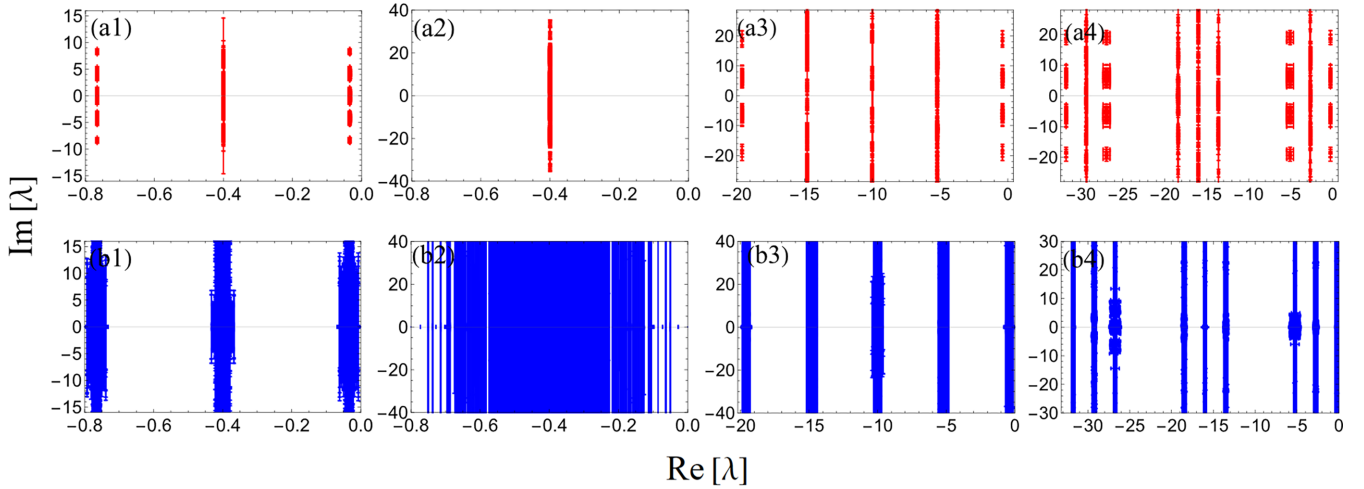$$X = \sum_{j=1}^{2N} s_j |\psi_{jR}\rangle\langle\psi_{jL}|, \tag{E11}$$

FIG. 10. The Liouvillian spectrum of odd channel (a1–a4) and even channel (b1–b4) with disorder strength $\delta = 0.1$ for systems with $N = 6$, and (a1, b1) $h = 0.3$, $\gamma = 0.2$, (a2, b2) $h = 3$, $\gamma = 0.2$, (a3, b3) $h = 3$, $\gamma = 5$, and (a4, b4) $h = 3$, $\gamma = 8$. The data are obtained by taking over 50 random configurations.

and get Eq. (E1) as

$$\Gamma(t) = \sum_{j,k=1}^{2N} \left[e^{(s_j + s_k)t} \langle \psi_{jL} | \Gamma(0) | \psi_{kL} \rangle | \psi_{jR} \rangle \langle \psi_{kR} | \right], \quad (E12)$$

in which $| \psi_{kL} \rangle = [\langle \psi_{kL} |]^T$, $\langle \psi_{kR} | = [| \psi_{kR} \rangle]^T$. So, the average magnetization is

$$
\begin{aligned}
\langle m^z(t) \rangle &= \left\langle \frac{1}{N} \sum_{j=1}^{N} \sigma_j^z(t) \right\rangle = -\frac{2i}{N} \sum_{j=1}^{N} \langle \hat{w}_{j,+} \hat{w}_{j,-} \rangle \\
&= \frac{1}{N} \sum_{j=1}^{N} (\Gamma_{N+j,j} - \Gamma_{j,N+j}) \\
&= \frac{1}{N} \text{Tr} \left(\begin{bmatrix} 0_N & I_N \\ -I_N & 0_N \end{bmatrix} \Gamma(t) \right), \quad (E13)
\end{aligned}
$$

where the matrix Γ of the initial state of all spin up is denoted as

$$\Gamma(0) = \begin{bmatrix} 0_N & -I_N/2 \\ I_N/2 & -iI_N \end{bmatrix}. \quad (E14)$$

APPENDIX F: STABILITY OF STRIPE STRUCTURE AGAINST RANDOM ONSITE DISORDER PERTURBATION

Here we demonstrate that the stripe structures are stable against random onsite disorder perturbation in the transverse field. The boundary-dissipated transverse field Ising model with transverse field strength being perturbed by random onsite disorder is described by

$$H = -J \sum_{j=1}^{N-1} \sigma_j^x \sigma_{j+1}^x - h_j \sum_{j=1}^{N} \sigma_j^z, \quad (F1)$$

where $h_j = h(1 + \delta_j)$ $(j = 1, 2, \ldots, N)$ is uniformly distributed in the interval $[h(1 - \delta), h(1 + \delta)]$, i.e., δ_j is a random number uniformly distributed in $(-\delta, \delta)$.

To see clearly how the disorder changes the structure of Liouvillian spectrum, we display the Liouvillian spectrum from the odd and even channels in Figs. 10(a1–a4) and 10(b1–b4), respectively. To compare with Fig. 1, we set the same parameters and the strength of the disorder as 10% ($\delta = 0.1$). It is shown that the structures of the stripes are still discernible even we introduce random onsite disorder, i.e., the spectrum structure is stable against random onsite disorder perturbation.

[1] H.-P. Breuer and F. Petruccione, *The Theory of Open Quantum Systems* (Oxford University Press, Oxford, UK, 2002).

[2] P. Schindler, M. Müller, D. Nigg, J. T. Barreiro, E. A. Martinez, M. Hennrich, T. Monz, S. Diehl, P. Zoller, and R. Blatt, Quantum simulation of dynamical maps with trapped ions, Nat. Phys. **9**, 361 (2013).

[3] H. Weimer, A. Kshetrimayum, and R. Orús, Simulation methods for open quantum many-body systems, Rev. Mod. Phys. **93**, 015008 (2021).

[4] G. Lindblad, On the generators of quantum dynamical semigroups, Commun. Math. Phys. **48**, 119 (1976).

[5] T. Prosen and M. Žnidarič, Matrix product simulations of nonequilibrium steady states of quantum spin chains, J. Stat. Mech.: Theory Exp. (2009) P02035.

[6] T. Prosen and I. Pižorn, Quantum Phase Transition in a Far-From-Equilibrium Steady State of an *XY* Spin Chain, Phys. Rev. Lett. **101**, 105701 (2008).

[7] T. Prosen, Third quantization: A general method to solve master equations for quadratic open Fermi systems, New J. Phys. **10**, 043026 (2008).

[8] T. Prosen, Exact Nonequilibrium Steady State of a Strongly Driven Open *XXZ* Chain, Phys. Rev. Lett. **107**, 137201 (2011).

[9] C. Guo and D. Poletti, Solutions for bosonic and fermionic dissipative quadratic open systems, Phys. Rev. A **95**, 052107 (2017).

[10] N. Shibata and H. Katsura, Dissipative spin chain as a non-Hermitian Kitaev ladder, Phys. Rev. B **99**, 174303 (2019).

[11] C. Guo and D. Poletti, Analytical solutions for a boundary-driven *XY* chain, Phys. Rev. A **98**, 052126 (2018).

[12] K. Yamanaka and T. Sasamoto, Exact solution for the Lindbladian dynamics for the open XX spin chain with boundary dissipation, SciPost Physics **14** 112, (2023).

[13] N. Shibata and H. Katsura, Quantum Ising chain with boundary dephasing, Prog. Theor. Exp. Phys. **2020**, 12A108 (2020).

[14] M. Žnidarič, Exact solution for a diffusive nonequilibrium steady state of an open quantum chain, J. Stat. Mech.: Theory Exp. (2010) L05002.

[15] M. Žnidarič, Relaxation times of dissipative many-body quantum systems, Phys. Rev. E **92**, 042143 (2015).

[16] S.-Y. Zhang, M. Gong, G.-C. Guo, and Z.-W. Zhou, Anomalous relaxation and multiple timescales in the quantum XY model with boundary dissipation, Phys. Rev. B **101**, 155150 (2020).

[17] B. Zhou, X. Wang, and S. Chen, Exponential size scaling of the Liouvillian gap in boundary-dissipated systems with Anderson localization, Phys. Rev. B **106**, 064203 (2022).

[18] S. Sachdev, *Quantum Phase Transitions* (Cambridge University Press, Cambridge, UK, 2000).

[19] E. Lieb, T. Schultz, and D. Mattis, Two soluble models of an antiferromagnetic chain, Ann. Phys. **16**, 407 (1961).

[20] S. Katsura, Statistical mechanics of the anisotropic linear Heisenberg model, Phys. Rev. **127**, 1508 (1962).

[21] P. Pfeuty, The one-dimensional Ising model with a transverse field, Ann. Phys. **57**, 79 (1970).

[22] A. Dutta, G. Aeppli, B. K. Chakrabarti, U. Divakaran, T. F. Rosenbaum, and D. Sen, *Quantum Phase Transitions in Transverse Field Spin Models: From Statistical Physics to Quantum Information* (Cambridge University Press, Cambridge, UK, 2015).

[23] M. V. Medvedyeva, F. H. L. Essler, and T. Prosen, Exact Bethe Ansatz Spectrum of a Tight-Binding Chain with Dephasing Noise, Phys. Rev. Lett. **117**, 137202 (2016).

[24] V. Popkov and C. Presilla, Full Spectrum of the Liouvillian of Open Dissipative Quantum Systems in the Zeno Limit, Phys. Rev. Lett. **126**, 190402 (2021).

[25] M. Nakagawa, N. Kawakami, and M. Ueda, Exact Liouvillian Spectrum of a One-Dimensional Dissipative Hubbard Model, Phys. Rev. Lett. **126**, 110404 (2021).

[26] B. Buča, C. Booker, M. Medenjak, and D. Jaksch, Bethe ansatz approach for dissipation: Exact solutions of quantum many-body dynamics under loss, New J. Phys. **22**, 123040 (2020).

[27] B. Zhu, R. Lü, and S. Chen, $\mathcal{PT}$ symmetry in the non-Hermitian Su-Schrieffer-Heeger model with complex boundary potentials, Phys. Rev. A **89**, 062102 (2014).

[28] Y.-N. Zhou, L. Mao, and H. Zhai, Rényi entropy dynamics and Lindblad spectrum for open quantum systems, Phys. Rev. Res. **3**, 043060 (2021).

[29] A. Jamiołkowski, Linear transformations which preserve trace and positive semidefiniteness of operators, Rep. Math. Phys. **3**, 275 (1972).

[30] M.-D. Choi, Completely positive linear maps on complex matrices, Linear Algebra Appl. **10**, 285 (1975).

[31] J. E. Tyson, Operator-Schmidt decompositions and the Fourier transform, with applications to the operator-Schmidt numbers of unitaries, J. Phys. A: Math. Gen. **36**, 10101 (2003).

[32] M. Zwolak and G. Vidal, Mixed-State Dynamics in One-Dimensional Quantum Lattice Systems: A Time-Dependent Superoperator Renormalization Algorithm, Phys. Rev. Lett. **93**, 207205 (2004).

[33] A. Kshetrimayum, H. Weimer, and R. Orús, A simple tensor network algorithm for two-dimensional steady states, Nat. Commun. **8**, 1291 (2017).

[34] W. P. Su, J. R. Schrieffer, and A. J. Heeger, Solitons in Polyacetylene, Phys. Rev. Lett. **42**, 1698 (1979).

[35] M. Klett, H. Cartarius, D. Dast, J. Main, and G. Wunner, Relation between $\mathcal{PT}$-symmetry breaking and topologically nontrivial phases in the Su-Schrieffer-Heeger and Kitaev models, Phys. Rev. A **95**, 053626 (2017).

[36] X. Z. Zhang and Z. Song, Geometric phase and phase diagram for a non-Hermitian quantum *XY* model, Phys. Rev. A **88**, 042108 (2013).

[37] C. Li, G. Zhang, X. Z. Zhang, and Z. Song, Conventional quantum phase transition driven by a complex parameter in a non-Hermitian $\mathcal{PT}$-ymmetric Ising model, Phys. Rev. A **90**, 012103 (2014).

[38] C.-X. Guo, C.-H. Liu, X.-M. Zhao, Y. Liu, and S. Chen, Exact Solution of Non-Hermitian Systems with Generalized Boundary Conditions: Size-Dependent Boundary Effect and Fragility of the Skin Effect, Phys. Rev. Lett. **127**, 116801 (2021).

[39] Z. Cai and T. Barthel, Algebraic Versus Exponential Decoherence in Dissipative Many-Particle Systems, Phys. Rev. Lett. **111**, 150403 (2013).

[40] T. Barthel, and Y. Zhang, Solving quasi-free and quadratic Lindblad master equations for open fermionic and bosonic systems, J. Stat. Mech. (2022) 113101.

[41] A. Alase, E. Cobanera, G. Ortiz, and L. Viola, Exact Solution of Quadratic Fermionic Hamiltonians for Arbitrary Boundary Conditions, Phys. Rev. Lett. **117**, 076804 (2016).